LA-10526-PR
Progress Report

Los Alamos National Laboratory is operated by the University of California for the United States Department of Energy under contract W-7405-ENG-36.

Space Nuclear Safety Program

April 1984

Los Alamos National Laboratory
Los Alamos, New Mexico 87545

DISCLAIMER

The four most recent reports in this series, unclassified, are LA-10134-PR, LA-10162-PR, LA-10190-PR, and LA-10511-PR.

This work was supported by the US Department of Energy, Office of Special Nuclear Projects.

Edited by Renate Lewin
Photocomposition by Ruth Steinberg

LA-10526-PR
Progress Report

LA--10526-PR

DE86 004374

UC-33A
Issued: October 1985

Space Nuclear Safety Program

April 1984

Compiled by
T. G. George

Los Alamos National Laboratory
Los Alamos, New Mexico 87545

SPACE NUCLEAR SAFETY PROGRAM
April 1984

Compiled by

T. G. George

ABSTRACT

This technical monthly report covers studies related to the use of $^{238}PuO_2$ in radioisotope power systems carried out for the Office of Special Nuclear Projects of the US Department of Energy by Los Alamos National Laboratory. Most of the studies discussed here are ongoing; results and conclusions described may change as the work continues.

I. GENERAL-PURPOSE HEAT SOURCE (GPHS)

A. Safety Verification Tests (SVTs)

1. Postmortem Examination of SVT-1 Through SVT-5 (D. Pavone). Microstructures of plutonia fuel pellets used in prime clads of test modules SVT-1 through SVT-5 are shown in Figs. 1-10. We attempted to select a sample that included the surface of the pellet and extended toward the core, but the extent of pellet breakup and the friability of pieces made it impossible to obtain such a sample in all instances.

The photomacrographs reveal a tendency toward reduced density near the surface in those samples of appropriate geometric shape. The HF-354 pellet sample (Fig. 7, SVT-4) was extensively fractured. Grain sizes in the individual pellets were generally similar; however, those of HF-354 were somewhat larger than average.

No second-phase, nonmetallic inclusions were observed, but a few metallic inclusions were present. The absence of nonmetallic inclusions correlates well with both the generally low level of impurities revealed by emission spectrographic analysis and the absence of vent effusate on the clad exteriors.

2. Postmortem Examination of SVT-6 (T. George). In SVT-6, a fully loaded GPHS module was impacted "side-on" (Fig. 11) at 54.6 m/s and 975°C. The fuel capsules had been aged for 90 days at 1287°C before being loaded into the test assembly. After loading, the test module was subjected to a temperature of 1375°C to simulate reentry. Encapsulation details for the SVT-6 clads are shown in Table I, and data describing the fuel pellets are given in Table II. After the test, a sealed catch tube containing the impacted module was transferred to Wing 2 of the CMR building.

The sealed catch tube was placed in an open-fronted hood and the pump-out plug was removed. A swab inserted into the pump-out hole registered <20,000 counts/min/cm^2. The end of the catch tube was removed, the inner nickel can (a radiation shield) was extracted with tongs, and the can/aeroshell/heat-source assembly was placed on a bed of solid CO_2. Even after extraction of the can/aeroshell/heat-source assembly, the catch tube contained a significant amount of debris—pulverized graphite, pieces of ceramic insulator, and bits of thermocouple wire (Fig. 12). After the largest pieces of graphite had been removed, the interior of the catch tube was washed and the contents were packaged for plutonium analysis.

Damage to the aeroshell was moderate (Fig. 13). The aeroshell walls fractured along the axial contact lines of graphite impact shell (GIS) A, 90° to the impact face; GIS A was released. Damage to the two GISs was significant (Figs. 14 and 15) but not unusual. Although the closure on GIS A opened, the fuel capsules were not released.

The fuel capsules were extracted from the GISs, photographed, and measured. Side and end views of each capsule are shown in Fig. 16. The capsule dimensions and calculated gross strains are listed in Tables III and IV.

TABLE I. Encapsulation Details for SVT–6 Fueled Clads

Capsule No.	SRP/NDT[a] Indication	Vent	Iridium Cup Weld Shield	Fuel Pellet
HF–189	13.3	P705-5	P705-3	8109HF189
HF–225	13.2	MER7–4	MER1–4	8111HF225
HF–361	4.4	PR725–5	PR726–1	8204HF361
HF–373	4.1	P803–6	PR272–3	8204HF373

[a]Savannah River Plant nondestructive testing.

TABLE II. Data for SVT–6 Fuel Pellets

Capsule No.	Fuel Pellet	Diameter (mm)	Length (mm)	Weight (g)	Fueled-Clad Processing Atm.
HF–189	8109HF189	27.4	27.5	148.8	Ar/O_2
HF–225	8111HF225	27.4	27.6	150.4	Ar/O_2
HF–361	8204HF361	27.5	27.6	150.3	Ar
HF–373	8204HF373	27.4	27.5	149.9	Ar

TABLE III. Dimensions of SVT–6 Fueled Clads

		HF–189	HF–225	HF–361	HF–373
Preimpact Dimensions (mm)					
Diameter		29.78	29.78	29.78	29.79
Length		30.00	30.00	30.00	29.98
Postimpact Dimensions (mm)					
Diameter					
Vent Cup	Min	28.01	28.09	26.62	25.34
	Max	30.94	31.34	32.93	32.50
Weld	Min	27.64	27.18	24.55	25.38
	Max	31.70	32.11	33.46	33.09
Blind Cup	Min	28.32	27.69	24.88	25.34
	Max	31.08	30.81	31.61	30.89
Length	Min	30.71	30.81	31.61	30.89
	Max	31.06	31.31	32.79	32.03

TABLE IV. Postimpact Strains (%) in the SVT-6 Fueled Clads

		HF-189	HF-225	HF-361	HF-373
Diameter					
Vent Cup	Min	−5.94	−5.67	−10.61	−14.94
	Max	+3.90	+5.24	+10.58	+9.10
Weld	Min	−7.11	−8.73	−17.56	−14.80
	Max	+6.45	+7.82	+12.36	+11.08
Blind Cup	Min	−5.20	−7.02	−16.45	−14.94
	Max	+4.36	+3.73	+9.13	+6.71
Length	Min	+2.37	+2.70	+5.37	+3.04
	Max	+3.53	+4.37	+9.30	+6.84

Macroscopic examination revealed that the primary capsules (HF-361 and HF-373) were severely deformed. Capsule HF-373 had breached (Fig. 17). The impact face contained a large axial crack (22.5 mm × 1.7 mm) and a smaller parallel crack (3.7 mm × 0.3 mm) on the vent-cup radius. Both cracks were apparently the result of fuel-fragment push-through. A large crease on the impact face of the HF-361 was also apparently caused by the differential displacement of large fuel fragments. Except for the large cracks in HF-373, the capsule surfaces were defect free; no weld cracks or other anomalies were observed on any of the capsules.

An abrasive cutting wheel was used to make a narrow circumferential slit 8–10 mm above the weld (blind cup) on capsules HF-189, HF-225, and HF-373. The capsules were pried open with a small screwdriver and the patterns of fuel fracture were photographed (Figs. 18–20). The capsules were then defueled.

To determine the quantity of respirable particles produced by the impact, we selected capsule HF-361 for a particle-size analysis. This capsule will be transferred to the glove-box train used for fines analysis and will be opened sometime in May.

Although preimpact radiographs (Figs. 21 and 22) showed little difference among fuel pellets (all of the pellets contained cracks), there was a noticeable difference between the fuel in capsule HF-373 and the fuel in capsules HF-189 and HF-225. Fuel in the trailing capsules (HF-189 and HF-225) was broken into small fragments that ranged in size from sand grains to pea gravel. The fuel in HF-373 was broken into massive fragments that were held tightly by the deformed clad. The fuel characteristics caused problems in obtaining samples for metallography and chemical analysis. The fuel in HF-189 and HF-225 tended to crumble, whereas the pieces removed from HF-373 were difficult to break into appropriately sized specimens. Although the differences in fuel character could have resulted from differences in capsule deformation, the fuel behavior would appear to reflect differences in processing.

B. DIRECT COURSE Recovery Operations (R. E. Tate)

In October 1983, the General Electric Company fielded a test that exposed a GPHS radioisotope thermoelectric generator (RTG) containing one simulant-fueled GPHS module to the blast of the DIRECT COURSE event at White Sands Missile Range. In this event, some 200 experiments were exposed at varying ranges to the detonation of 609 tons of ammonium nitrate/fuel oil explosive. The RTG was mounted on a 119.7-ft tower 56.5 ft from the explosive sphere center (39.0 ft from the sphere surface) to simulate the geometry of the space shuttle's external tank and RTG. The temperature of the simulant-fueled module and the adjacent dummy modules was maintained at 1100°C through shot time by power from a battery bank. The test was designed to provide information on the effects of a propellant explosion on the RTG, should one occur at shuttle launch.

The blast damaged the simulant-fueled clads to a much greater extent than had been anticipated. Iridium fragments were recovered 1000 ft out, over a path about 250 ft wide. Some fragments were located between ground zero and the RTG tower. Fortunately, the iridium clads had been mildly irradiated to form relatively short-lived ^{192}Ir, making the fragments easier to locate and recover. About 100 fragments of iridium, approximately three-fourths of the cladding material, were recovered by a team from the Advanced Nuclear Technology Group at Los Alamos. The team members used sensitive delta-rate meters, which easily located the small pieces of iridium.

After the test, questions were raised concerning the dispersal of the UO_2 (^{238}U) fuel simulant. In the last week in February, four months after the DIRECT COURSE event, we returned to White Sands Missile Range to map uranium distribution in the RTG impact area.

A rectangle 200 ft × 500 ft was staked out on the DIRECT COURSE test bed to cover most of the area

where iridium clad fragments had previously been recovered. The long-dimension midline of this rectangle coincided with the ground zero/RTG tower base radial on a magnetic azimuth of 122° (Fig. 23). The rectangle was divided into a grid of 20 ft × 20 squares, with the zero x-coordinate located at −50 ft on the 122° radial. We discovered the remnants of the shot and RTG towers and recorded their locations. Surface samples were collected at the 286 grid intersection points at 600, 700, 800, 900, 1000, and 1100 ft along the radial and 1000 ft north and south of the radial at $x = 500$ feet. Gamma-ray spectra were also recorded at about two-thirds of the grid points. We were unable to collect gamma-ray data at all grid points because of an instrument failure.

Using a uniform collection technique, a team from the Physical Metallurgy Group at Los Alamos collected the surface soil samples. Much of the collection area had been compacted by heavy equipment during test-bed construction; therefore collecting surface samples was a challenge. Soil was collected from an area about 6 in. square, to a depth of about ⅜ in. The soil was ground to break up all hard clumps and was put through a 10-mesh sieve. Stones and debris <10 mesh were discarded after visual inspection. The <10-mesh material was transferred to two high-purity polyethylene containers, one a special 4-mℓ vial used subsequently for reactor irradiation and the other a 25-mℓ bottle for a back-up sample. The sample containers were marked with six-digit numbers to indicate the grid-point origin.

The soil samples were submitted for neutron activation analysis at the Los Alamos Omega West Research Reactor, using automated equipment developed by the Isotope and Nuclear Chemistry Division for the National Uranium Resource Evaluation (NURE) program. The polyethylene vials containing the 4- to 5-g soil samples were transferred pneumatically through stations that (1) weighed the container and sample, (2) irradiated the sample in the reactor neutron flux for 20 s, and (3) counted the delayed fission neutrons from ^{235}U for 30 s immediately upon removal from the reactor. A computer print-out listed the sample number (grid point location), sample weight, neutron counts, flux normalization, and uranium content in parts per million to two decimal places. The depleted-uranium fuel simulant contains only 0.2 percent ^{235}U rather than the 0.7 percent in naturally occurring uranium. However, the neutron analysis technique is very sensitive to even trace quantities of ^{235}U, so the results give a good indication of uranium distribution over the DIRECT COURSE test bed. The results of the analyses are plotted as a computer-generated contour map in Fig. 23.

Ten samples, seven from the highest levels identified by neutron activation analysis and three from the farthest background areas, were reexamined by a technique that activated the ^{238}U. In this method of analysis, neutron capture creates ^{239}U, which decays to ^{239}Np, a gamma emitter that is easily identified. Table V compares uranium concentrations obtained by the two techniques.

To evaluate the uranium content over a significantly larger area at each grid point and to look specifically for ^{238}U, a team from the Advanced Nuclear Technology Group at Los Alamos analyzed the gamma-ray spectra at the grid points. The team used three units with hyperpure germanium detectors mounted on tripods; the gamma-ray spectra were analyzed with portable 1000-channel units. Counting time at each grid point was 5 min.

To distinguish ^{238}U from the GPHS–RTG and the ^{238}U in the background, we had planned to look for the enhancement of some gamma ray produced early in the ^{238}U decay chain, specifically the 1001-keV line from ^{234}Pa decay, relative to a gamma ray produced later in

TABLE V. Uranium Concentration at Selected Points Determined by Two Activation Methods

	Method		
Grid Point	^{235}U Fission (ppm)	^{238}U Activation (ppm)	Comments
120,200	3.63	4.23	—
140,100	2.59	3.60	Adjacent to 23-g iridium recovery
140,120	2.54	3.41	
160,100	2.70	4.23	
240,120	3.09	3.39	—
260,140	3.81	6.48	—
360,040	4.04	3.48	—
500,1000	2.51	<4.4	background
500,−1000	2.34	2.43	background
1100,100	2.30	2.82	background

the chain, specifically the 619-keV line from ^{214}Bi decay. However, these measurements were only partially successful because the 1001-keV line proved to be all but invisible in the spectra taken. This invisibility is attributed not only to the possibility of wide ^{238}U dispersal, but also to the ^{40}K in the background. The radiation from ^{40}K led to a Compton shoulder, which raised the continuum near the 1001-keV peak.

Data were acquired only at about two-thirds of the grid points because of recurring failures in the tape units of the spectrum analyzers. However, nowhere among the grid points studied were there more than a very few grams of ^{238}U within 3–5 ft of the germanium detectors.

The gamma-ray spectra analysis technique was considerably more successful in locating residual ^{192}Ir. About 23 g of iridium, some of it buried 10 in. deep, was recovered from a location (140,110) between grid points. The ^{192}Ir was clearly visible in the spectra at adjoining grid points 10 ft away. Various outlying points also showed ^{192}Ir in their spectra, although the concentrations were much less. The ^{192}Ir at (140,110) was easily located with delta-rate meters. The germanium detectors helped demonstrate that concentrations of radioactivity located with delta-rate meters were due to ^{192}Ir and not to ^{238}U. Searches for uranium with only delta-rate meters would have produced erroneous results because uncollected iridium fragments were still present.

Conclusion. Los Alamos personnel attempted to obtain the dispersal pattern or "footprint" of ^{238}U fuel simulant released from the GPHS–RTG exposed to the DIRECT COURSE explosion. However, ^{238}U is a singularly difficult radionuclide to map because of its low specific activity and the very small branching ratio for gamma rays that are easy to detect, and because ^{238}U occurs naturally in the background. The mapping that was done and the rather wide dispersal of the iridium fuel cladding suggest that no large pieces of the simulant fuel survived the DIRECT COURSE explosion and that the fuel simulant was finely divided and widely dispersed.

II. SAFETY TECHNOLOGY PROGRAM

A. Biaxial Testing (T. George)

In this month we impacted two DOP-26 iridium disks. Both disks were tested at 1440°C and 45 m/s in a +,0 strain state. One disk (ZR572-1) was heat-treated to produce an average of 5 grains/0.635-mm thickness, and the other disk (ZR576-8) was heat-treated to give an average of 15 grains/0.635-mm thickness. Unfortunately, the punch penetration used in both tests was insufficient; although both disks were badly orange peeled, neither disk fractured. We intend to repeat these tests in May, and we will also heat-treat and impact six additional DOP-26 disks and eight DOP-26 tensile specimens.

B. Iridium Chemistry (K. Axler and D. Peterson)

Ternary phases present along the grain boundaries of iridium used for cladding nuclear heat sources are a potential cause of embrittlement. In this month we investigated Th/Ir/C and Th/Ir/P ternary compounds.

We arc-melted a mixture of Th, Ir, and C in an attempt to prepare a ternary. A button was obtained that contained Th/C and Th/Ir phases, but no ternary phases were evident during x-ray diffraction analysis.

We also heated a mixture of Th, Ir, and P at 900°C in an evacuated quartz ampule in an attempt to prepare a ternary phase. The mixture was pressed into a pellet and was heated in one-day stages, at 100° intervals, from 600°–900°C. The sample components appeared to interact and form a reddish material that was submitted for x-ray analysis.

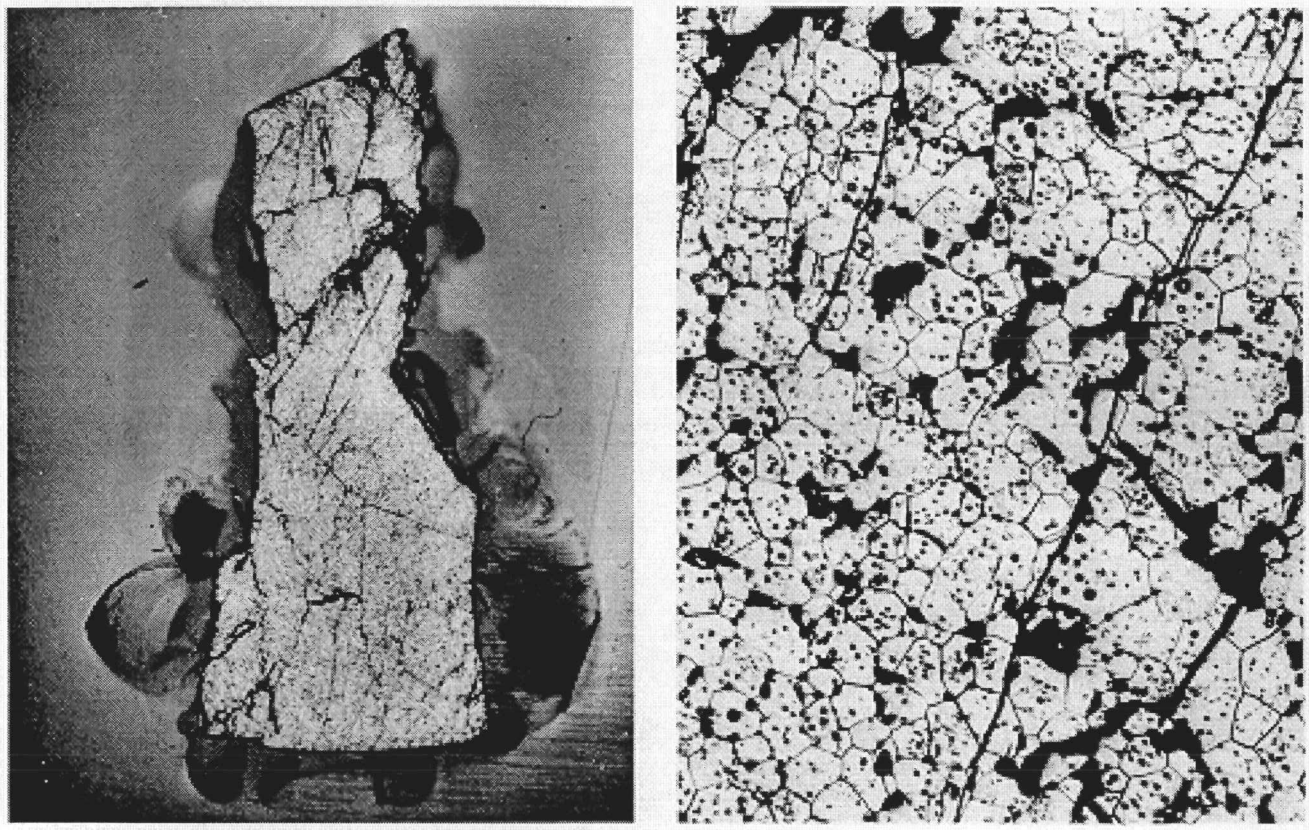

(a) (b)

Fig. 1. Microstructure of plutonia pellet HF-232. (a) 10×, (b) 250×.

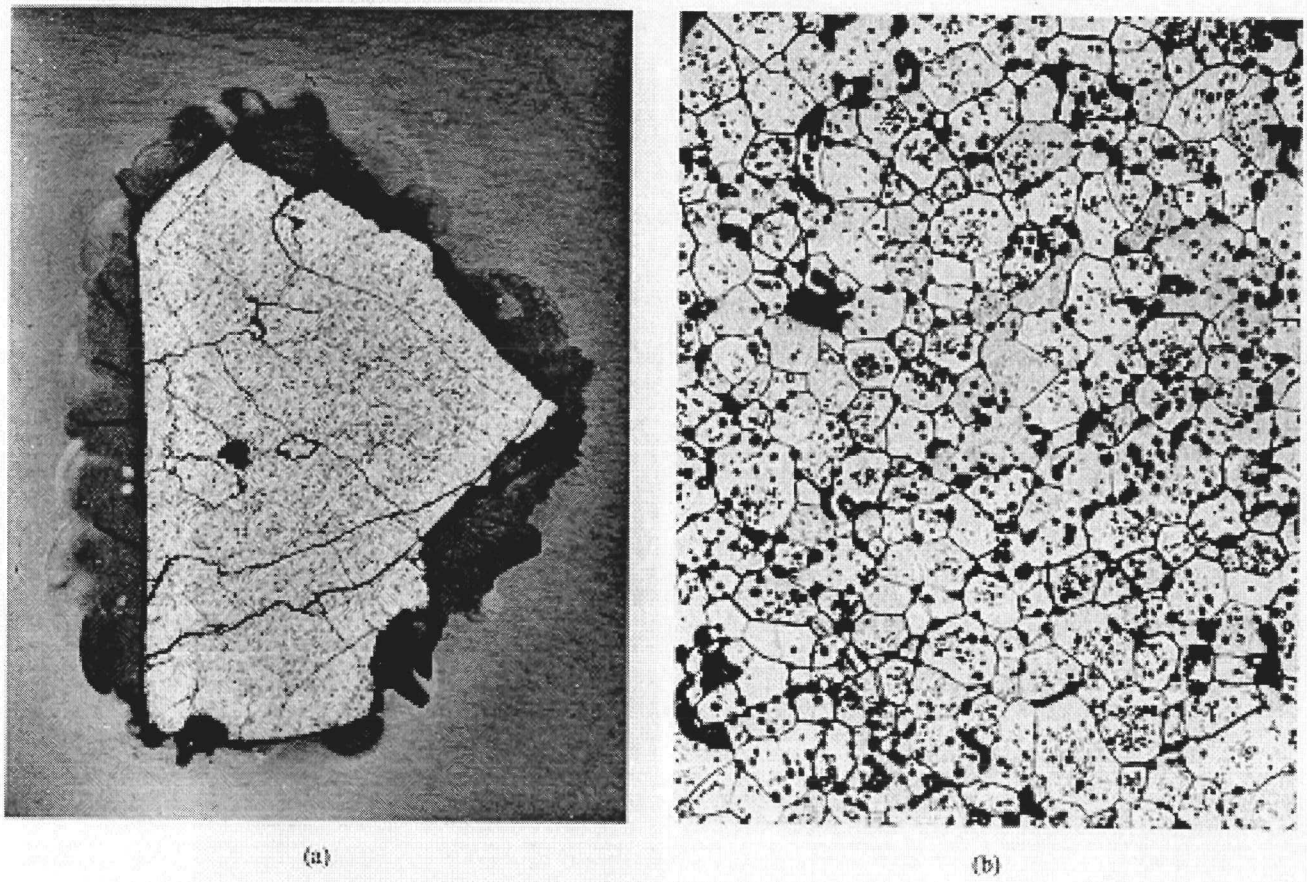

(a) (b)

Fig. 2. Microstructure of plutonia pellet HF–238. (a) 10×, (b) 100×.

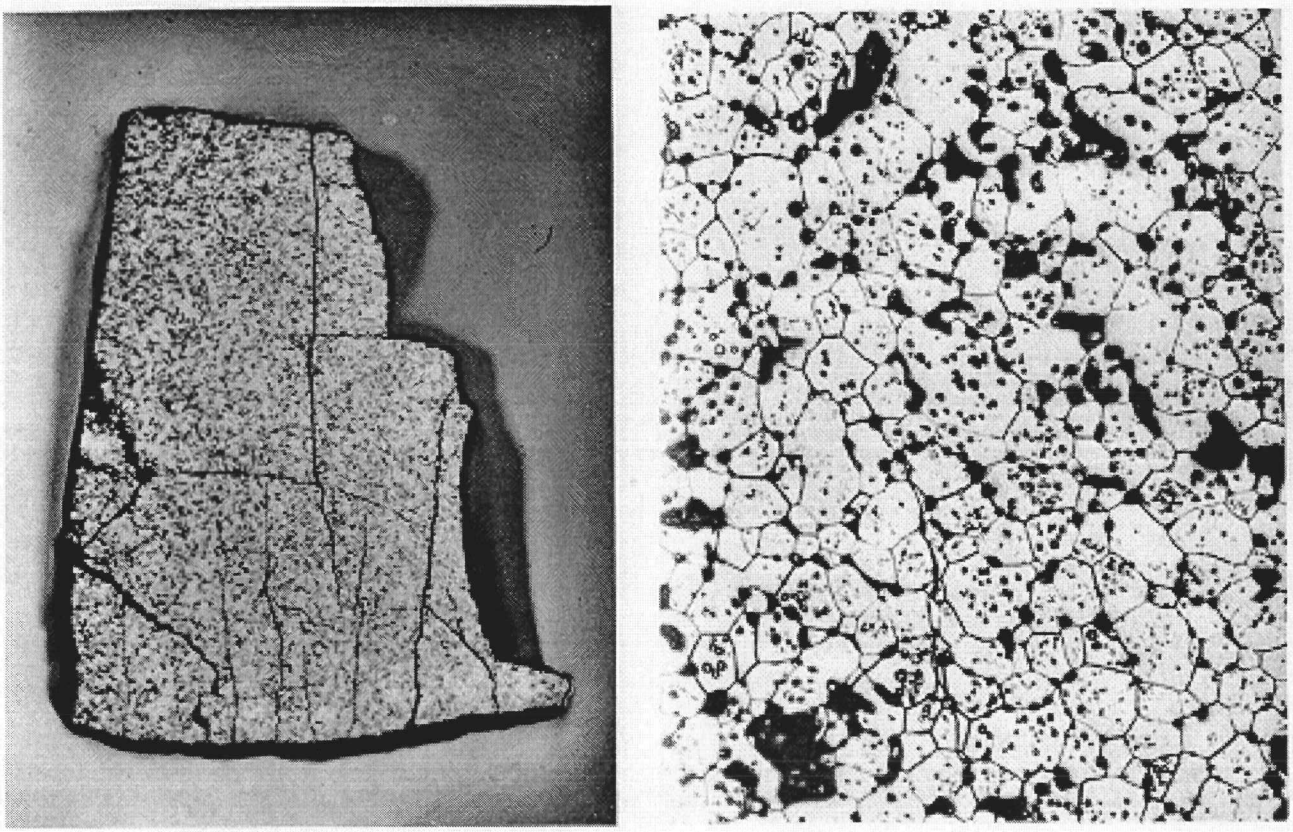

(a) (b)

Fig. 3. Microstructure of plutonia pellet HF-335. (a) 10×, (b) 250×.

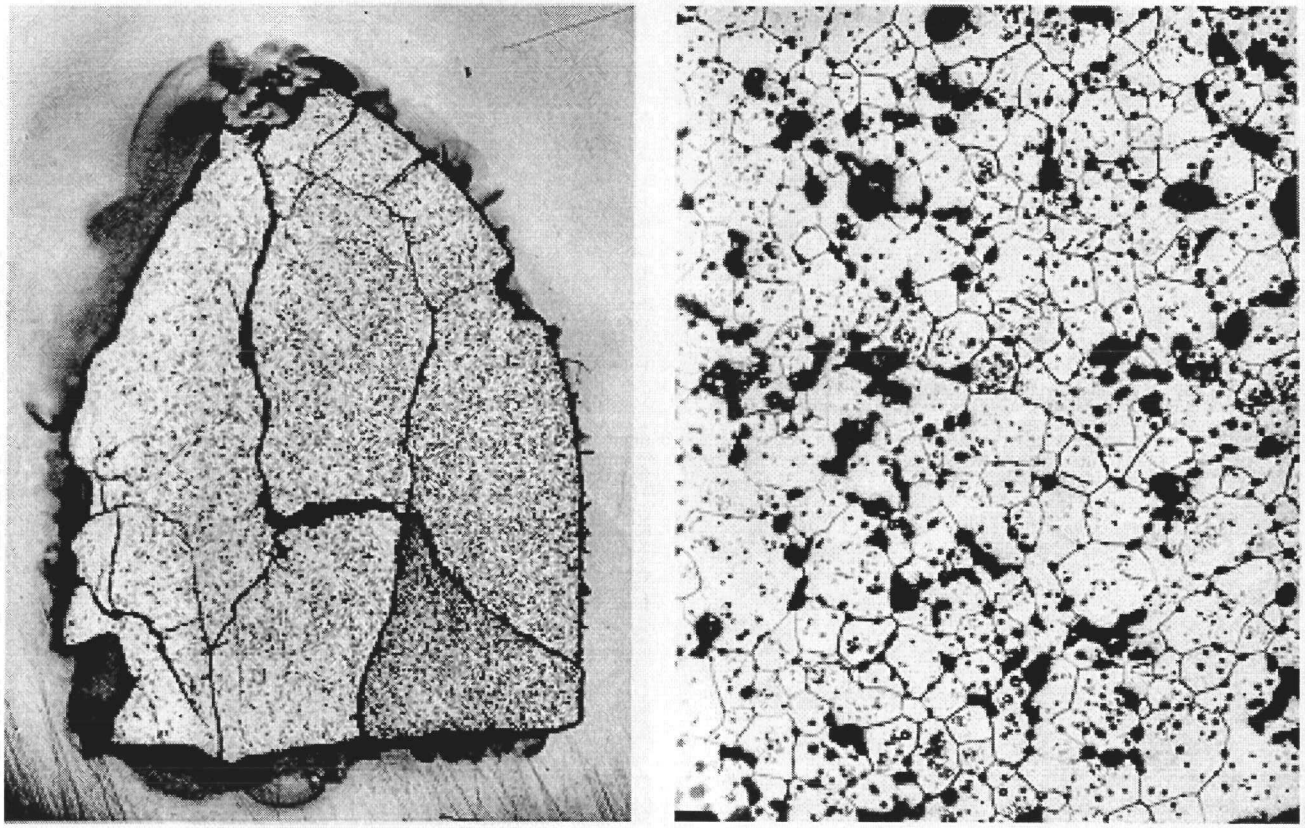

(a) (b)

Fig. 4. Microstructure of plutonia pellet HF–369. (a) 10X, (b) 250X.

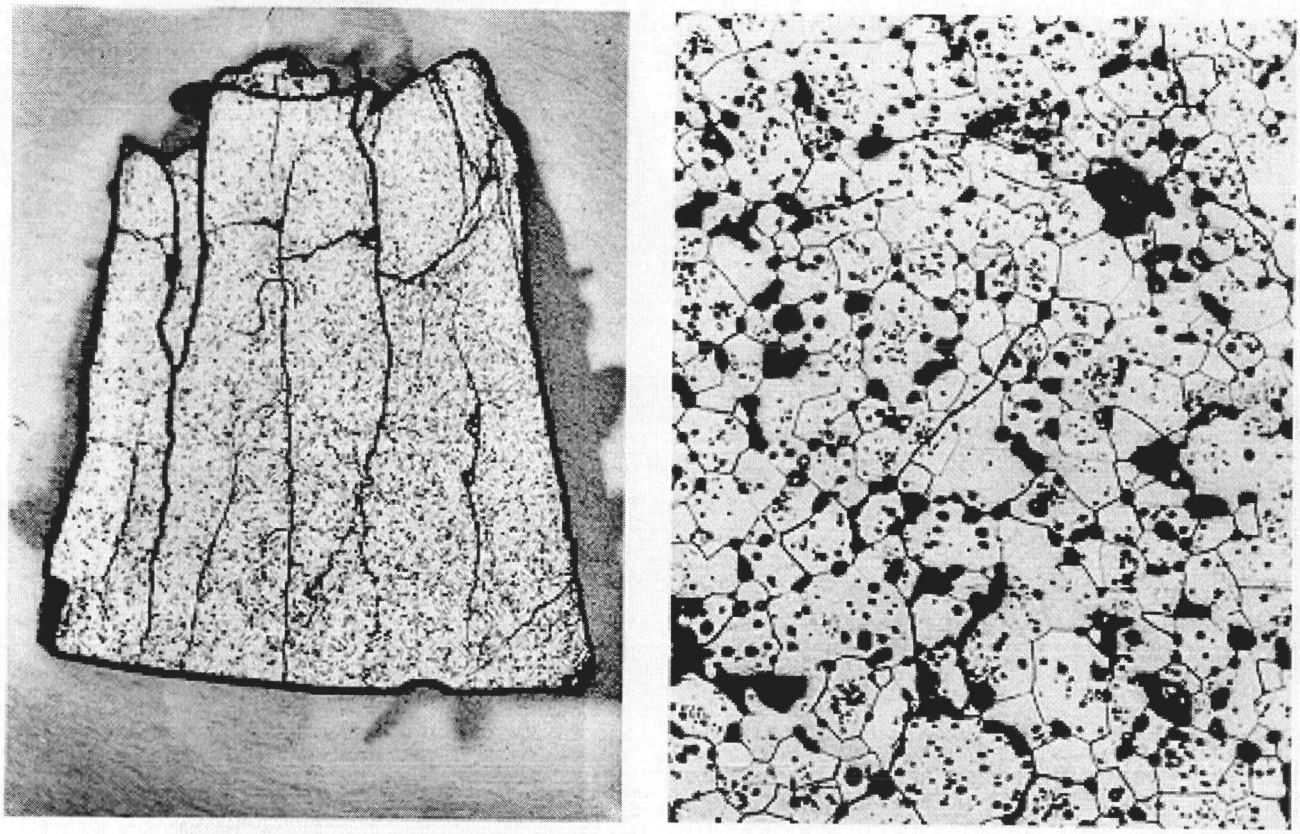

(a) (b)

Fig. 5. Microstructure of plutonia pellet HF–350. (a) 10×, (b) 250×.

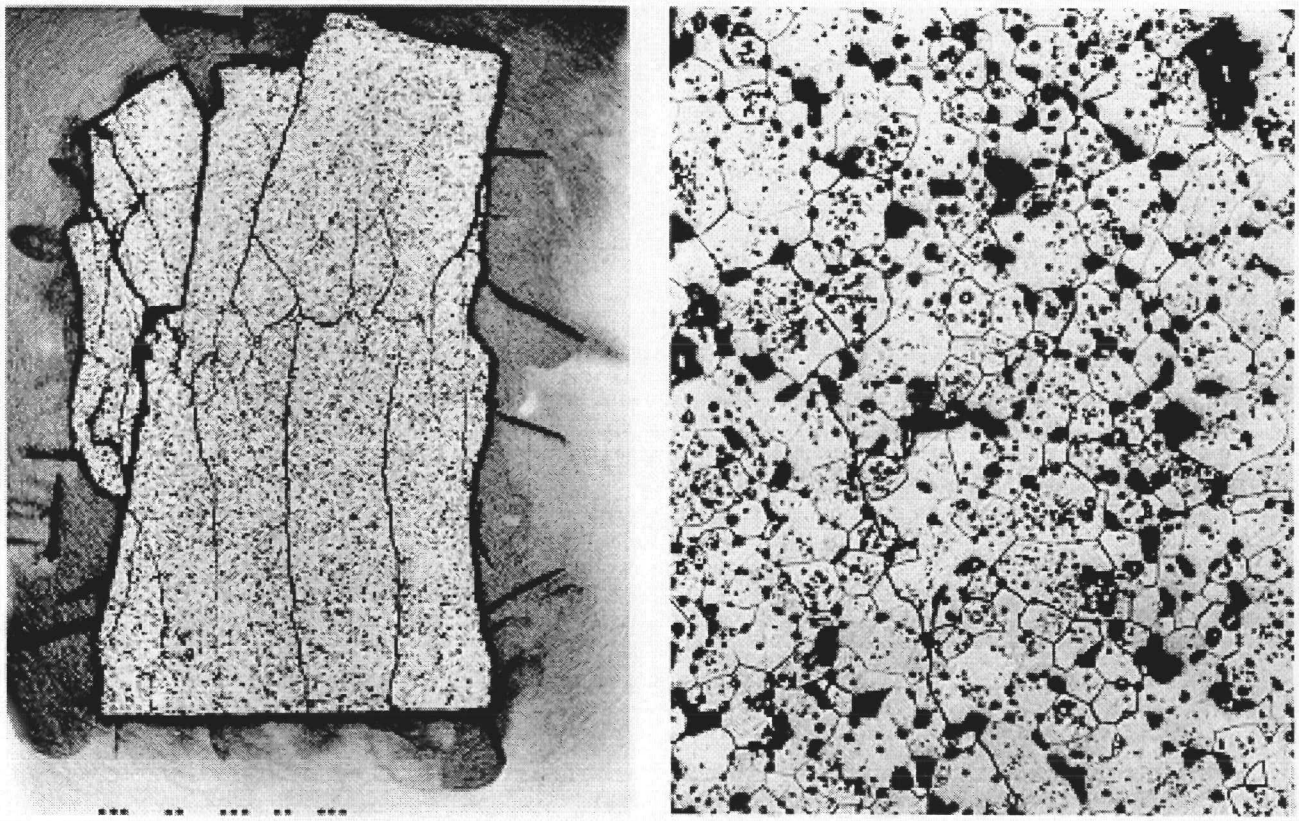

(a) (b)

Fig. 6. Microstructure of plutonia pellet HF-345. (a) 100X, (b) 250X.

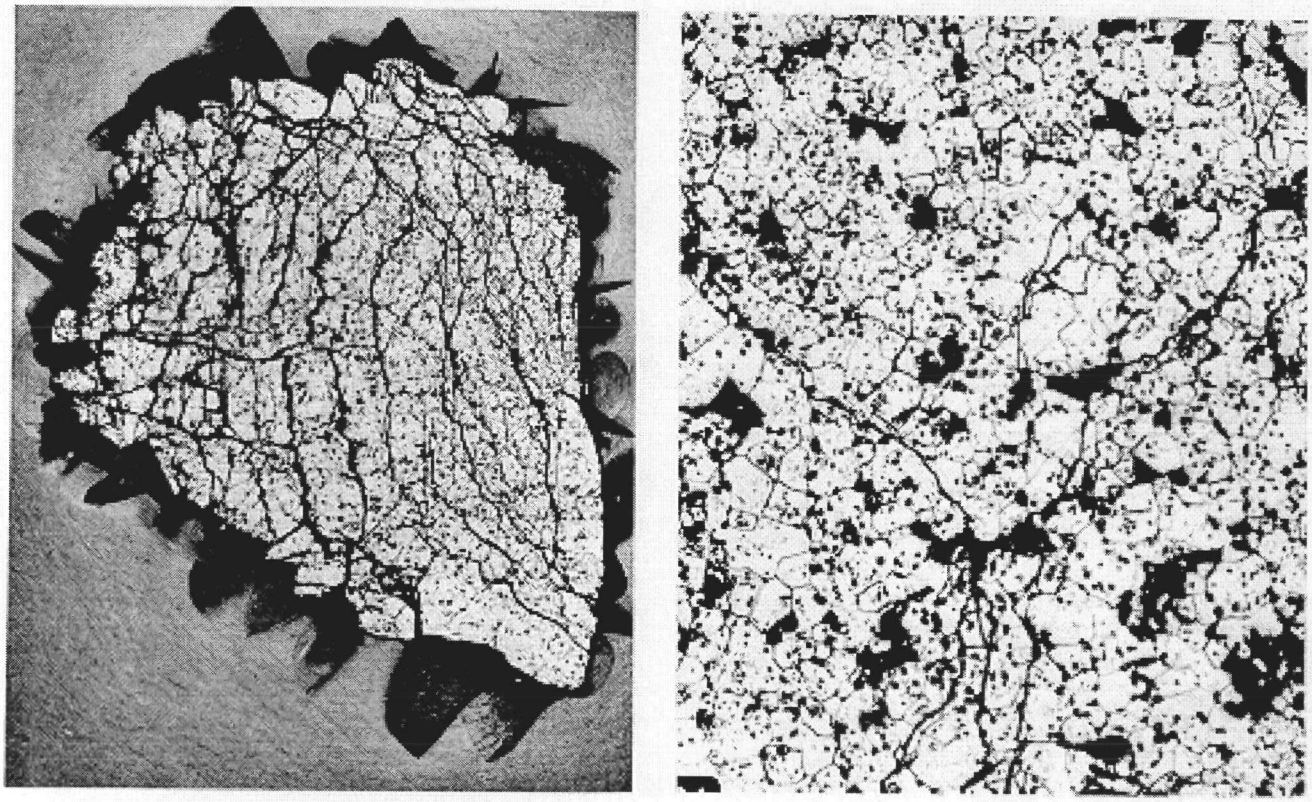

(a) (b)

Fig. 7. Microstructure of plutonia pellet HF-354. (a) 10×, (b) 250×.

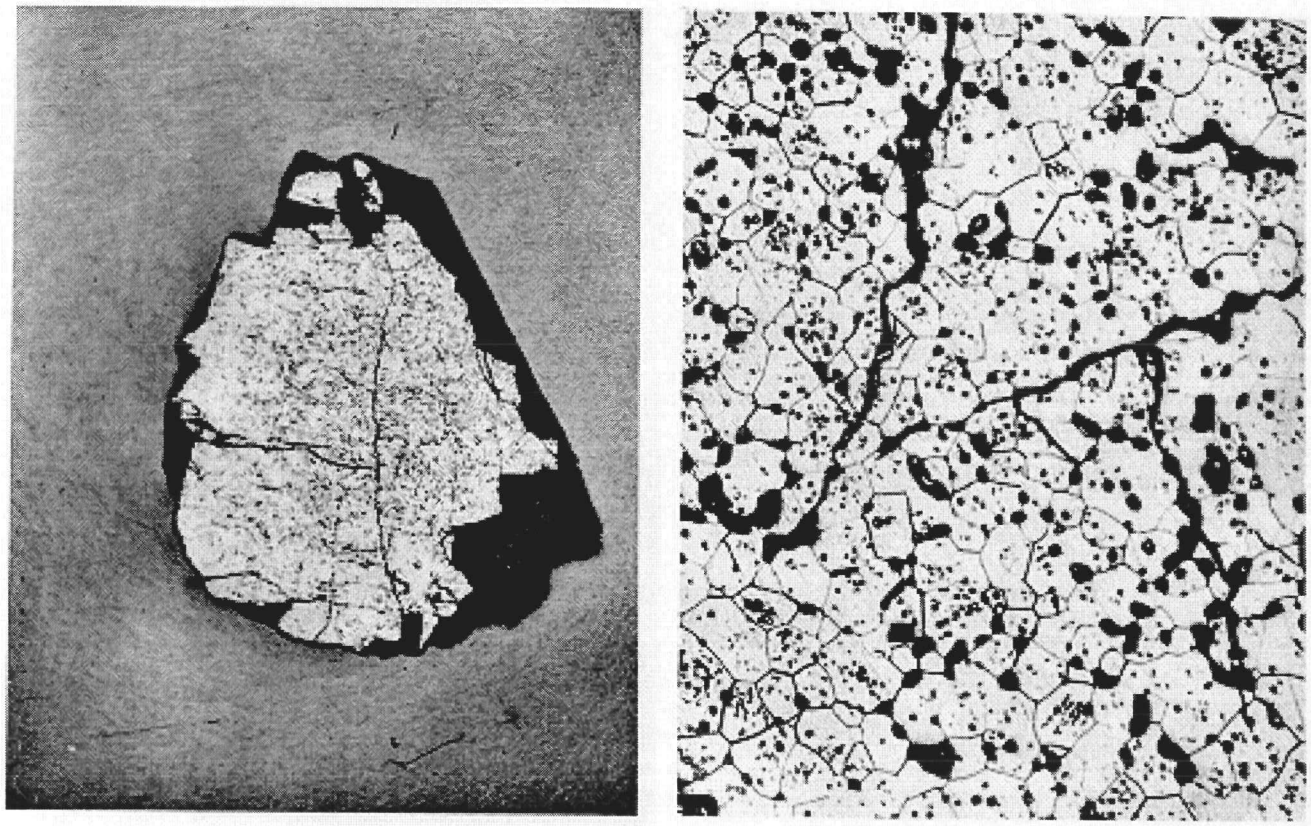

(a) (b)

Fig. 8. Microstructure of plutonia pellet HF–348. (a) 10×, (b) 250×.

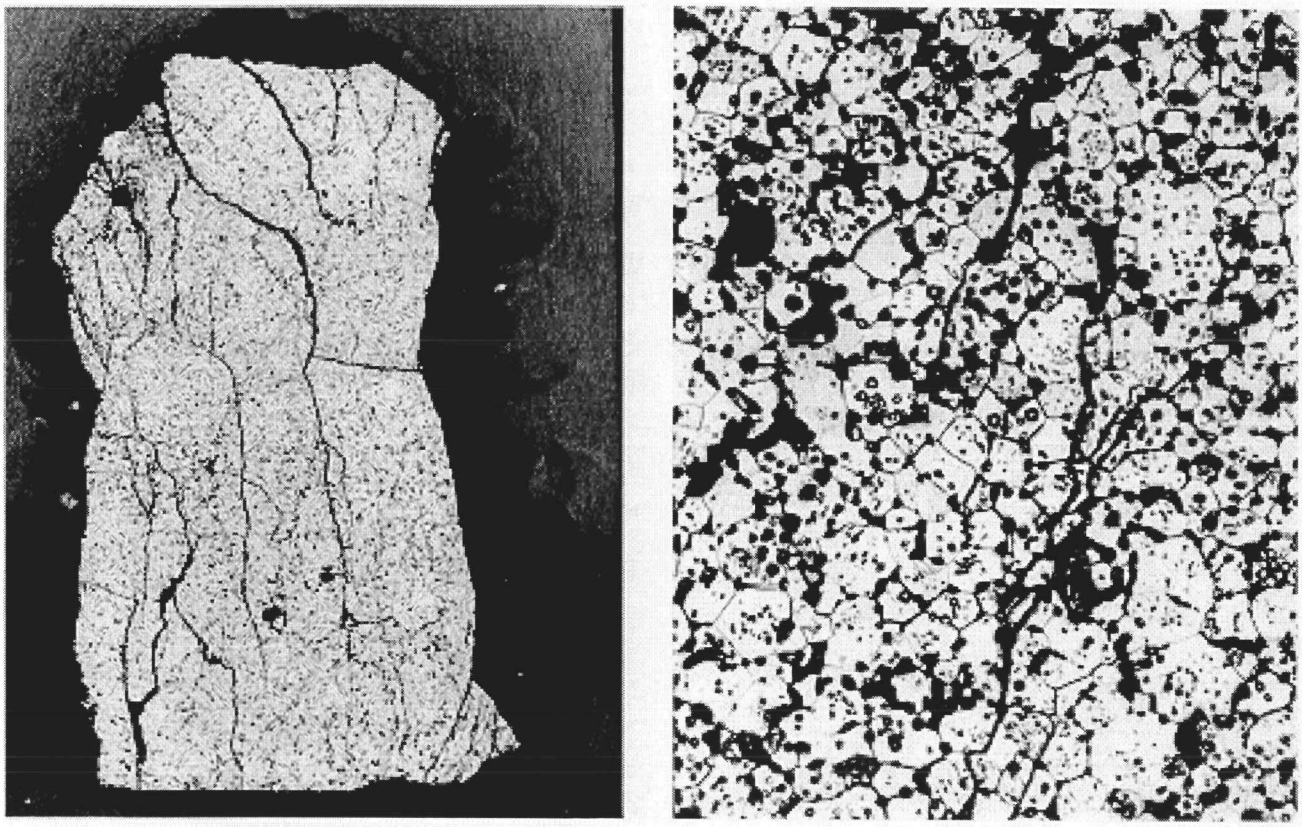

(a) (b)

Fig. 9. Microstructure of plutonia pellet HF–260. (a) 10×, (b) 250×.

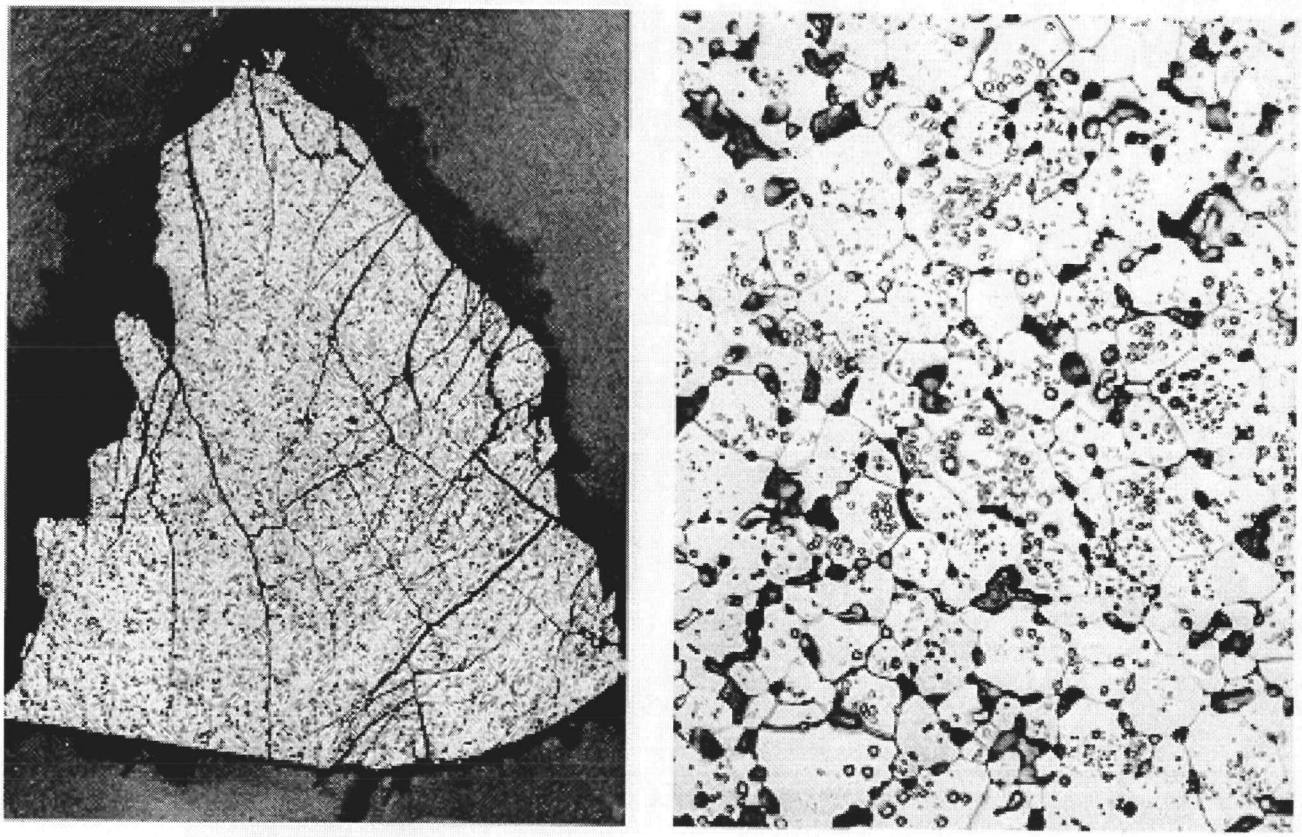

(a) (b)

Fig. 10. Microstructure of plutonia pellet HF-267. (a) 10X, (b) 250X.

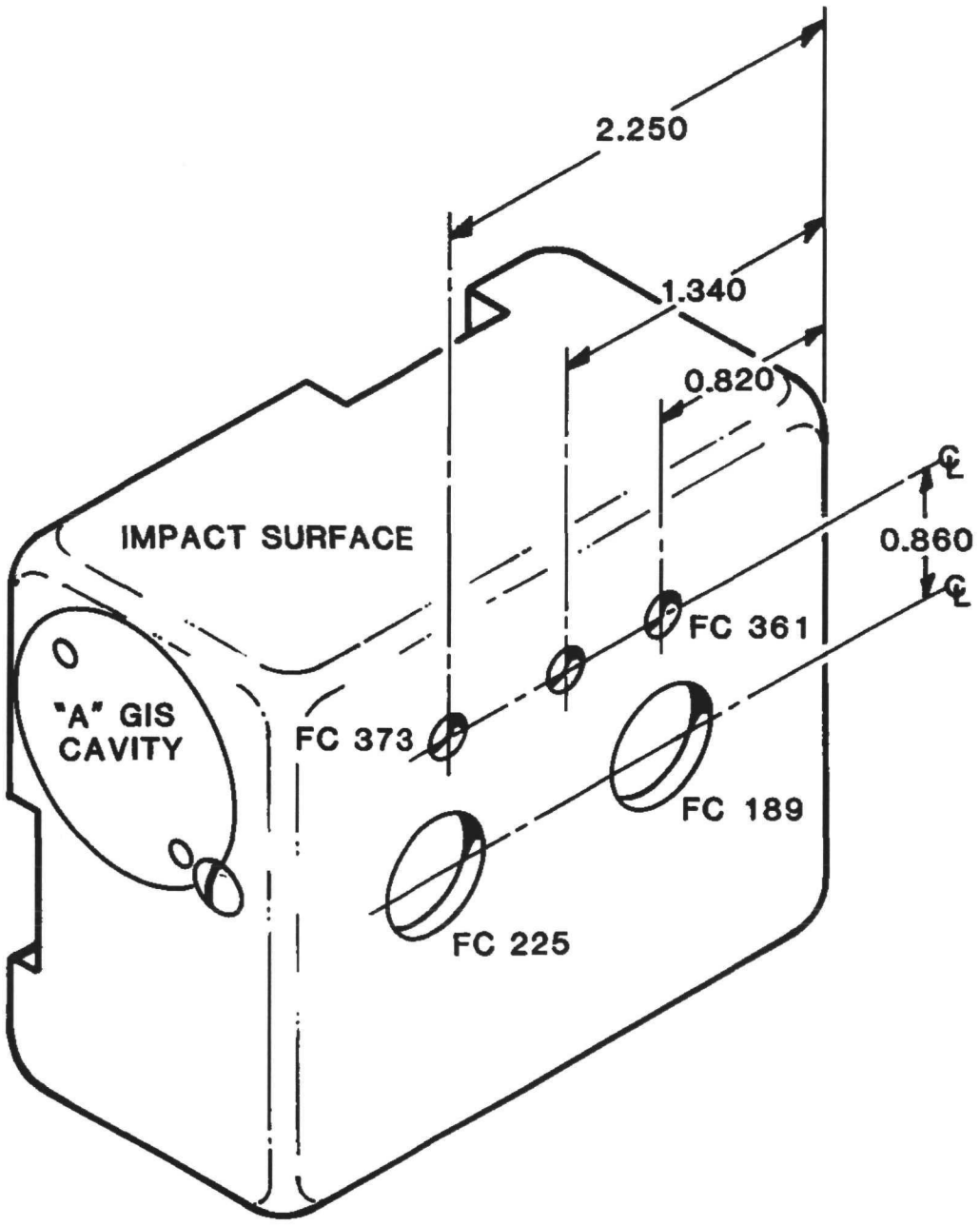

Fig. 11. The SVT-6 test module was impacted "side-on" at 54.6 m/s and 975°C.

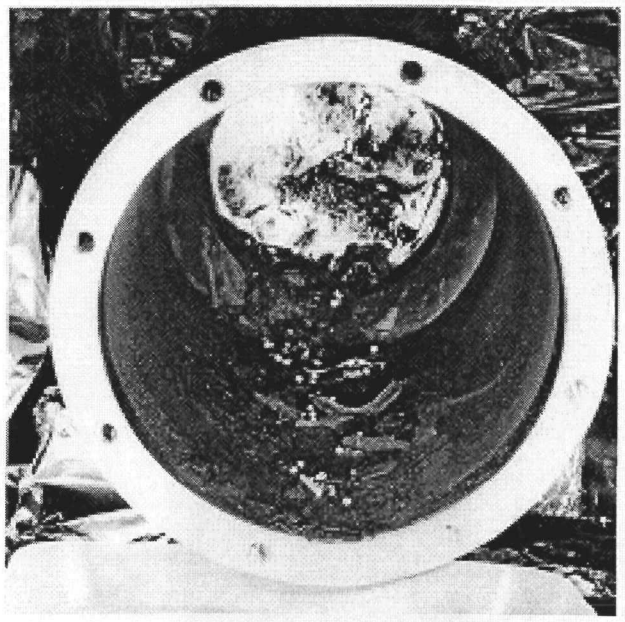

Fig. 12. A significant amount of debris remained in the catch tube after extraction of the can/aeroshell/heat source assembly; 0.25×.

Fig. 13. Damage to the SVT-6 aeroshell was moderate; 0.25×.

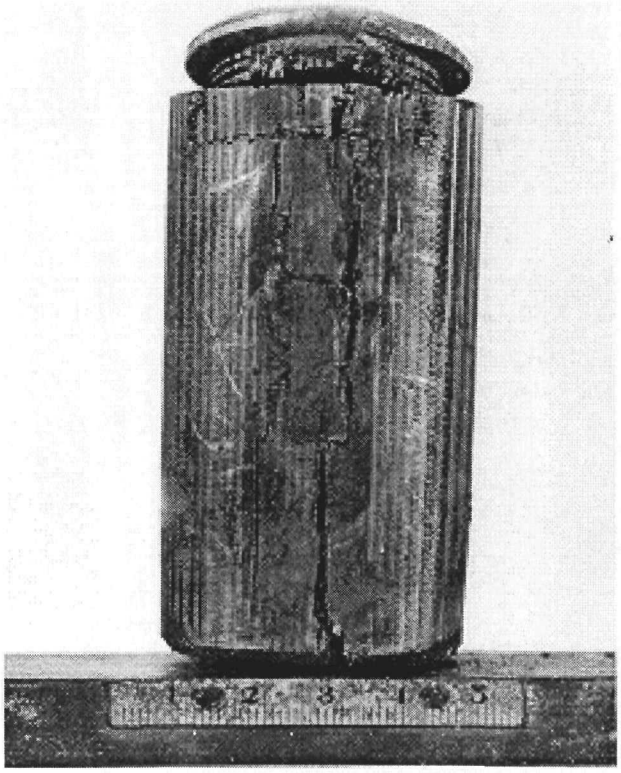

(a)

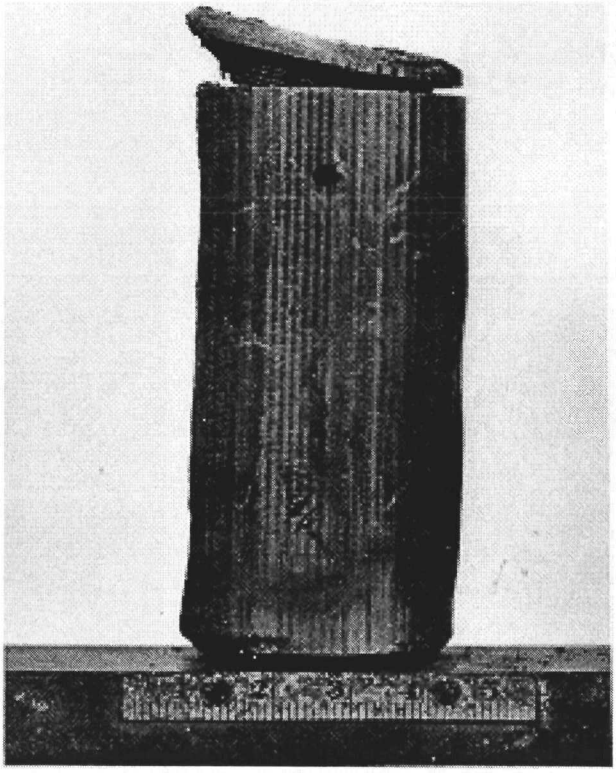

(b)

Fig. 14. Although the closure on GIS A opened, the fuel capsules were not released. (a) Impact face and (b) profile; both at 1×.

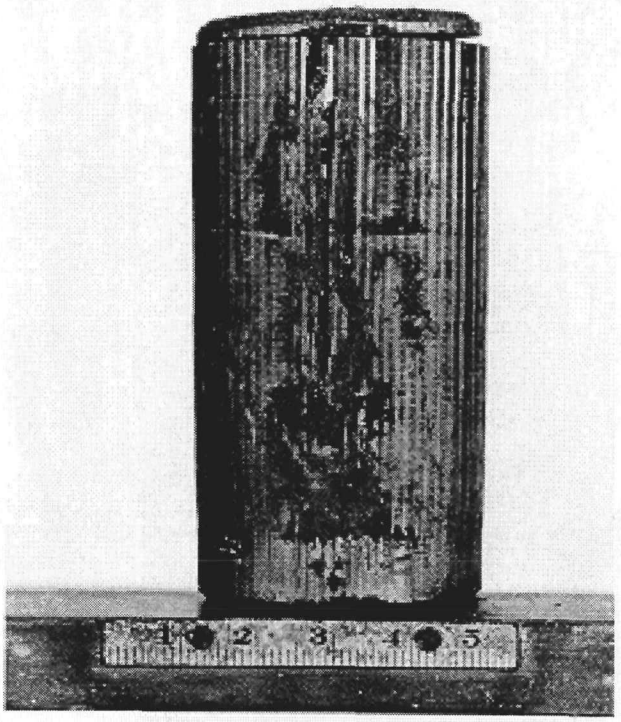

(a)

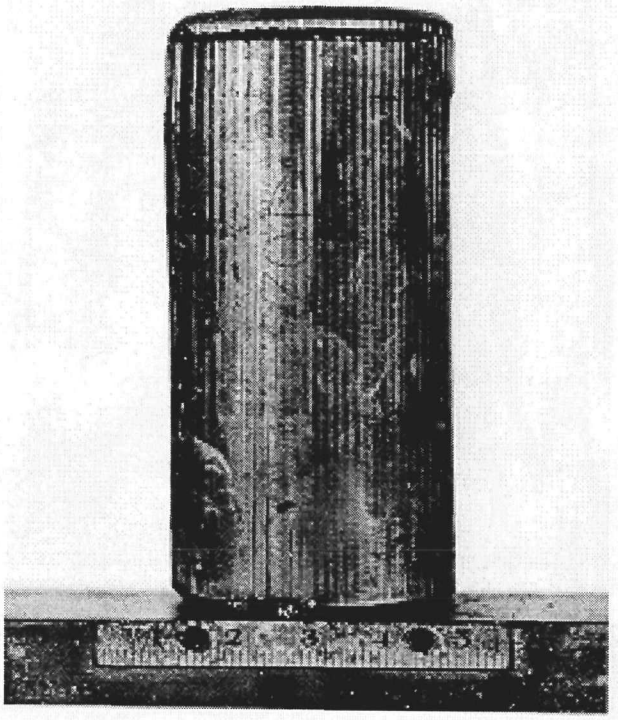

(b)

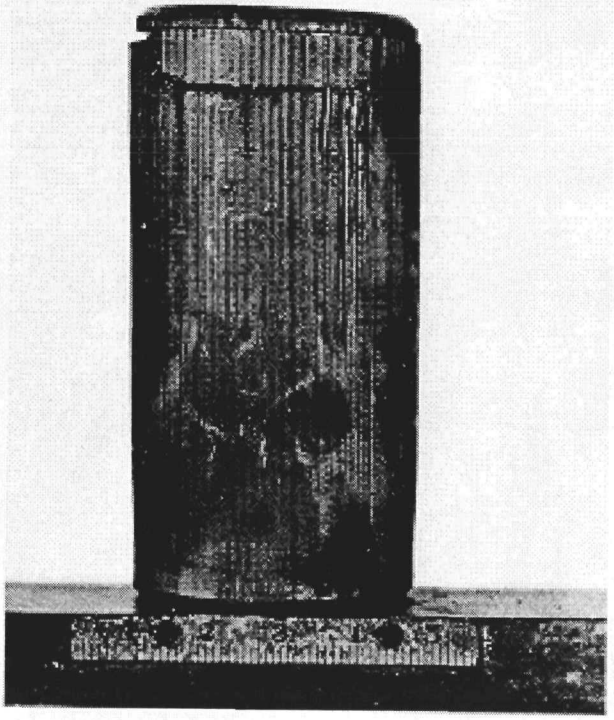

(c)

Fig. 15. GIS B survived the impact with only moderate deformation. (a) Impact face, (b) profile, and (c) back side. All at 10×.

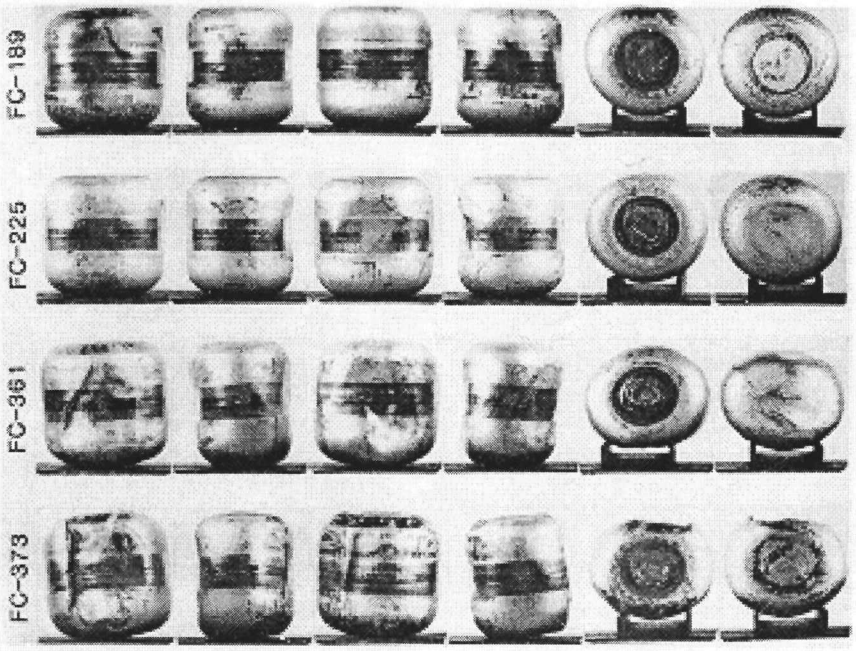

Fig. 16. Postimpact macrographs of the SVT-6 capsules. The impact face of each capsule is shown in the far left column; in each succeeding view the capsule is rotated 90°. The last two columns are end views. All at 0.35×.

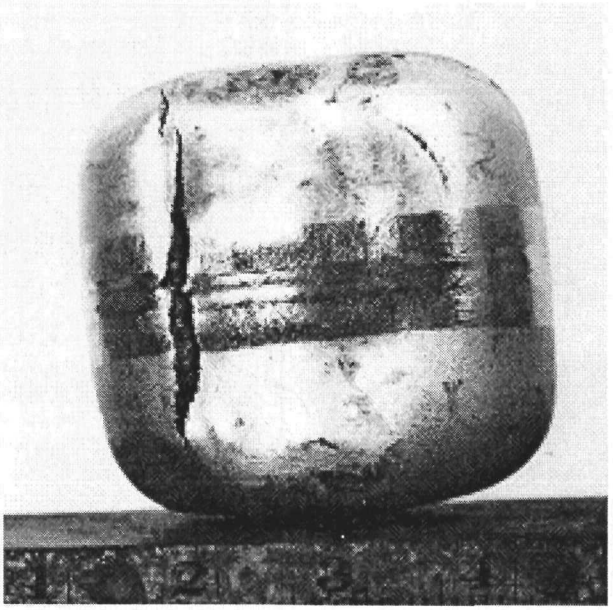

Fig. 17. The impact face of capsule HF-373 was traversed by two cracks; 2×.

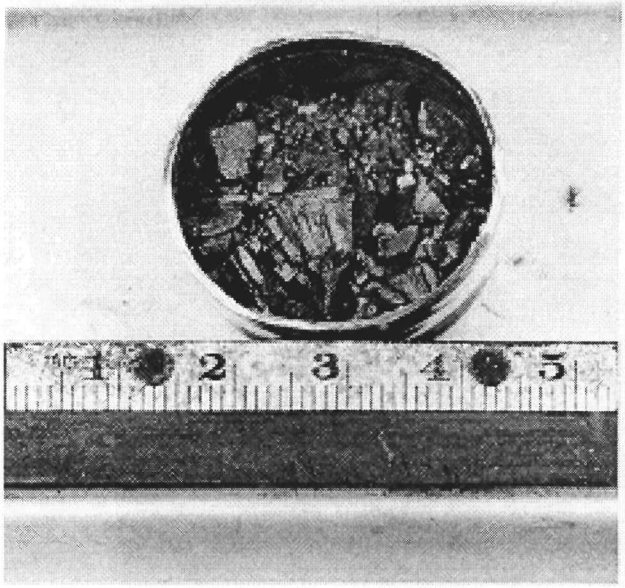

Fig. 18. The fuel in capsule HF-189 had a sand-like consistency; 1.5×.

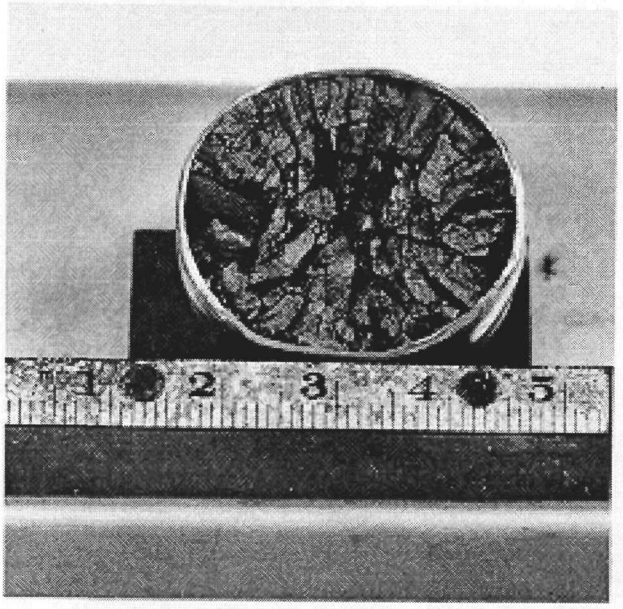

Fig. 19. The fuel in capsule HF-225 broke into gravel-sized chunks; 1.5×.

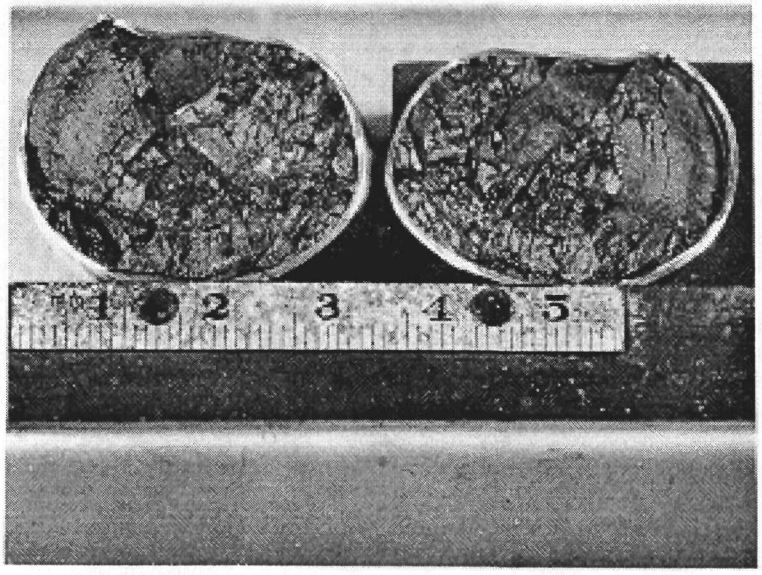

Fig. 20. The fuel in capsule HF-373 was broken into massive fragments; 1.5×.

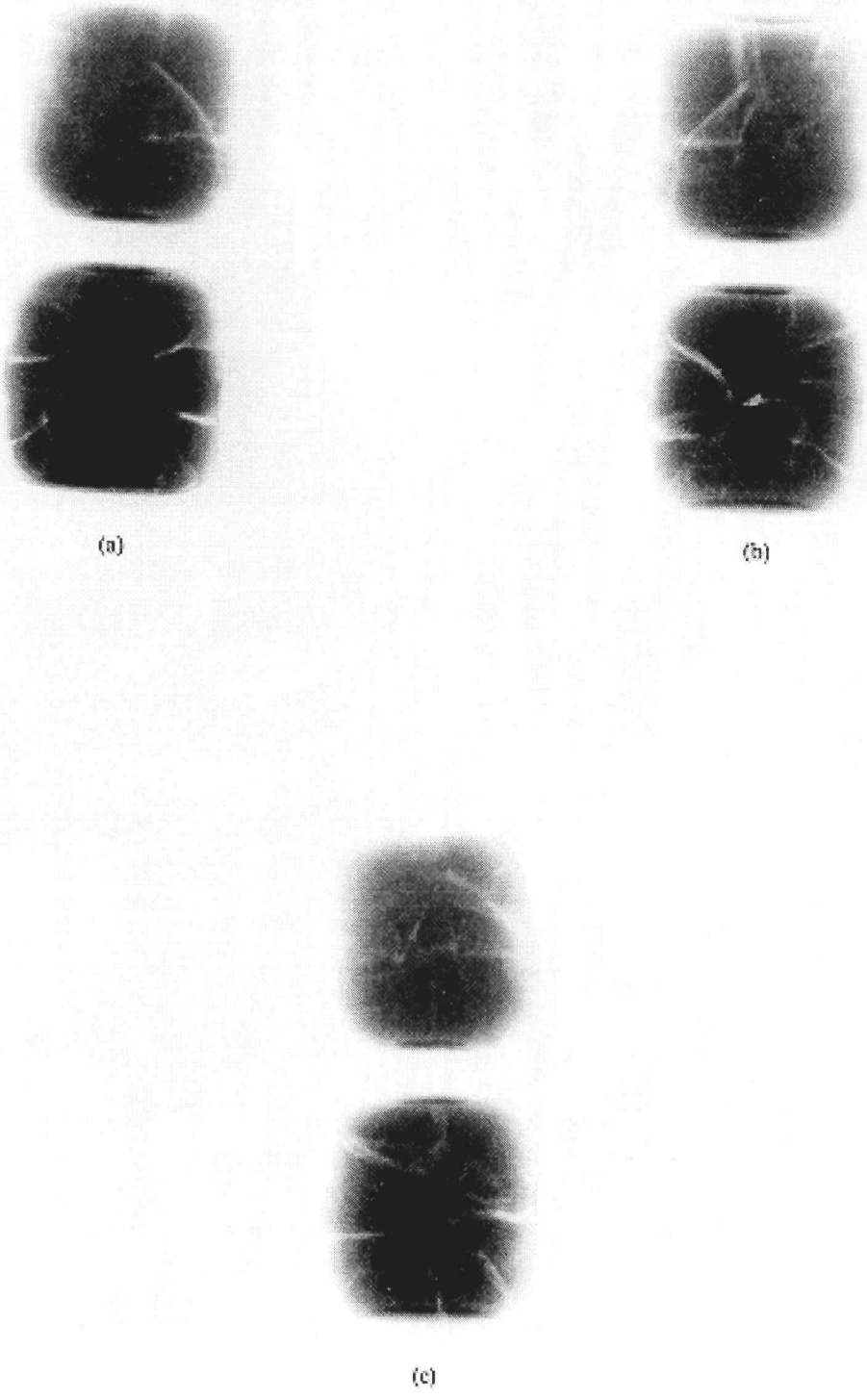

Fig. 21. Radiographs of the fuel pellets in GIS A, taken after the recent heat treatment. HF–361 is at top, and HF–373 is in the bottom position. (a) At 0°, (b) turned 120°, and (c) turned 240°. All at 1X.

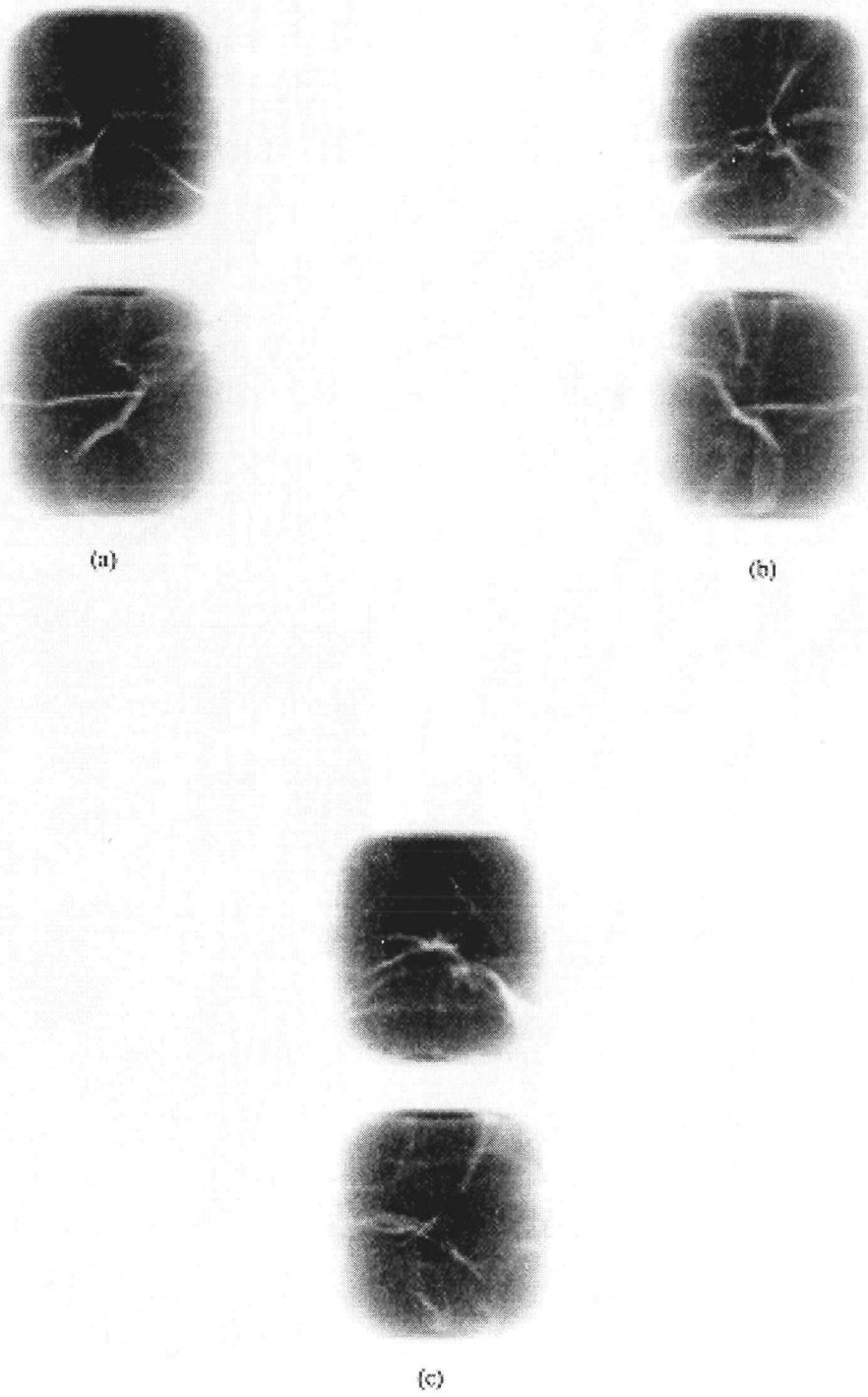

Fig. 22. Radiographs of the fuel pellets in GIS B, taken after the recent heat treatment. HF-189 is at the top, and HF-225 is in the bottom position. (a) At 0°, (b) turned 120°, and (c) turned 240°. All at 1×.

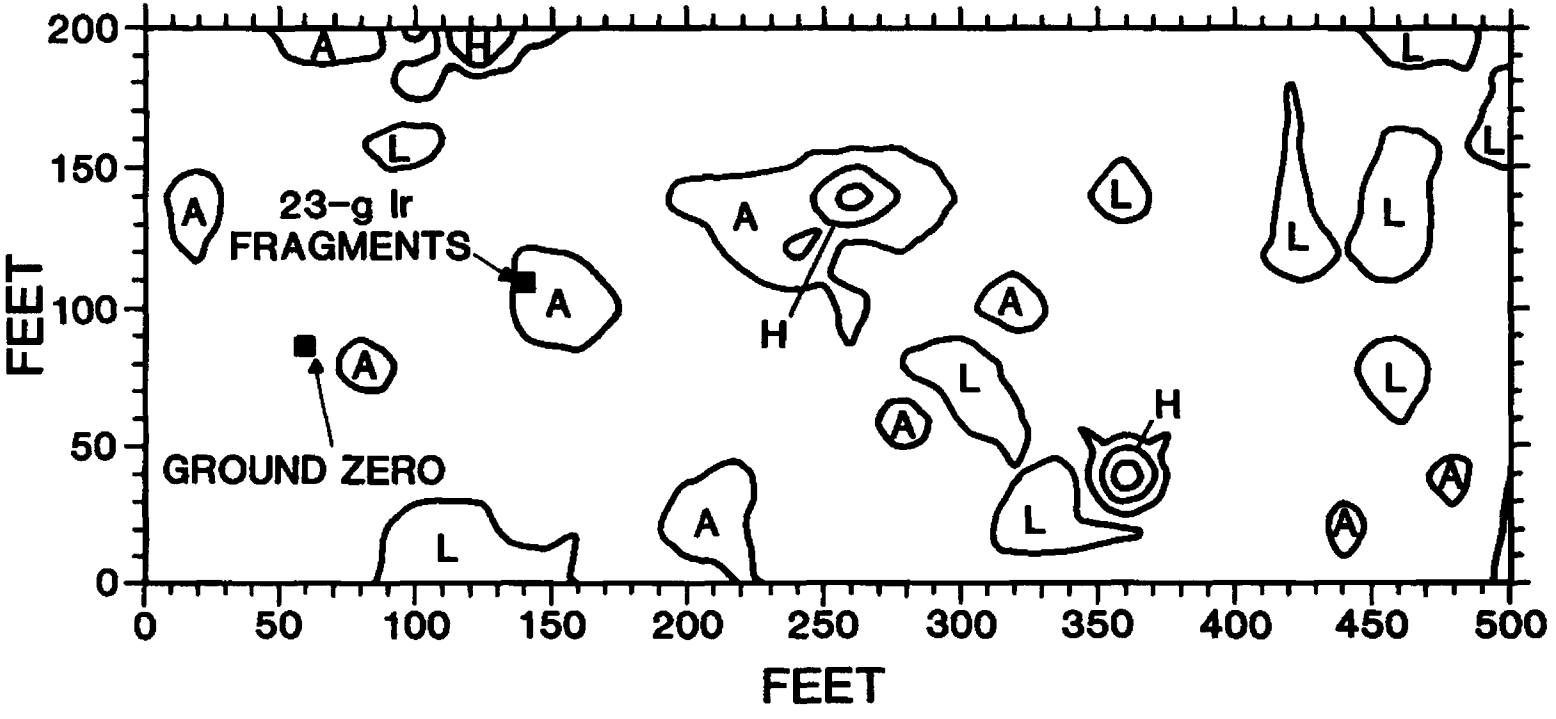

Fig. 23. Uranium distribution at the DIRECT COURSE test site. Contours: Background = 2.0–2.5 ppm U; L (low) = 1.5–2.0 ppm U; A (above) = 2.5–3.0 ppm U; H (high) = 3.0–4.0 ppm U.

ADDITIONAL DISTRIBUTION

B. J. Rock, Dept. of Energy/OSNP, Washington, DC
G. L. Bennett, Dept. of Energy/OSNP, Washington, DC
J. J. Lombardo, Dept. of Energy/OSNP, Washington, DC
R. B. Morrow, Dept. of Energy/OSNP, Washington, DC
R. Brouns, Dept. of Energy/OSNP, Washington, DC
J. Griffo, Dept. of Energy/OSNP, Washington, DC
D. K. Stevens, Dept. of Energy/BES, Washington, DC
M. Norin, Dept of Energy, Washington, DC
N. P. Klug, Dept. of Energy, Washington, DC
L. Smith, Dept. of Energy, Washington, DC
E. Bjoro, Dept. of Energy, Washington, DC
G. H. Ogburn, Dept. of Energy, Washington, DC
J. A. Yoder, Dept. of Energy, Washington, DC
C. Osterberg, Dept. of Energy, Washington, DC
I. Van Der Hoven, Dept. of Energy, Rockville, MD
J. V. Dorigan, Dept. of Energy, Washington, DC
W. O. Forster, Dept. of Energy, Washington, DC
R Watters, Dept. of Energy, Washington, DC
H B. Rosenthal, Dept. of Energy, Washington, DC
Col. Terry Hawkins, ATSD (AE), Dept of Defense, Washington, DC
Lt. Col. Jim Greening, HQ USAF/IG, Dept of Defense, Washington, DC
D. L. Foster, Dept. of Energy, Albuquerque, NM
J. P. Crane, Dept. of Energy, Albuquerque, NM
K. Elliot, Dept. of Energy, Albuquerque, NM
D. L. Krenz, Dept. of Energy, Albuquerque, NM
J. R. Roeder, Dept. of Energy, Albuquerque, NM
R B Crouch, Dept. of Energy, Albuquerque, NM
J. N. Bailey, Dept. of Energy, Albuquerque, NM
H. N. Hill, Dept of Energy/DOA, Miamisburg, OH
L. C. Sjostrom, Dept. of Energy, Aiken, SC
S. W. Ahrends, Dept. of Energy/ORO, Oak Ridge, TN
R. J. Hart, Dept. of Energy/ORO, Oak Ridge, TN
J. Pidkowicz, Dept. of Energy, Oak Ridge, TN
W L. Von Flue, Dept. of Energy, SFOO, Oakland, CA
T. B. Kerr, NASA, Washington, DC
F. R. Schmidt, NASA, Washington, DC
E. Gabris, NASA, Washington, DC
N. Sculze, NASA, Washington, DC
B. R. McCullar, NASA, Washington, DC
Operations Space Shuttle, NASA, Washington, DC
A. V. Diaz, NASA, Washington, DC
R. G. Ivanoff, Jet Propulsion Laboratory, Pasadena, CA
R. W. Campbell, Jet Propulsion Laboratory, Pasadena, CA
L. C. Montgomery, Jet Propulsion Laboratory, Pasadena, CA
L. T. Shaw, Jet Propulsion Laboratory, Pasadena, CA
R. J. Spehalski, Jet Propulsion Laboratory, Pasadena, CA
Dr. Agnus D. McRonald, Jet Propulsion Laboratory, Pasadena, CA
P. Jaffe, Jet Propulsion Laboratory, Pasadena, CA
AFWL/SNS, Attn: Col. J. A. Richardson, Kirtland AFB, NM
AFWL/NTYNS, Attn: Capt. D. E. Zimmerman, Kirtland AFB, NM
Lt. Col. James H. Lee, Jr., AFWL/NTYN, Kirtland AFB, NM
Capt. Michael K. Seaton, AFWL/NTYNP, Kirtland AFB, NM
Col John Joyce, AFISC/SND, Kirtland, AFB, NM
Maj. John Rice, AFISC/SNA, Kirtland AFB, NM
P. Dick, Teledyne Energy Systems, Timonium, MD
M. Goldman, University of California, Davis, CA
C. Smith, Sandia National Laboratories, Albuquerque, NM
R. L. Hannigan, Sandia National Laboratories, Albuquerque, NM
R. Harner, Sandia National Laboratories, Albuquerque, NM
C. M. Barnes, L. B. Johnson Space Center, NASA, Houston, TX
R. H. Brown, L. B. Johnson Space Center, NASA FM, Houston, TX
R. G. Rose, L. B. Johnson Space Center, NASA FA, Houston, TX
Harold Battaglia, L. B. Johnson Space Center, NASA PF, Houston, TX
W. H. Boggs, NASA, DE-A, J. F. Kennedy Space Center, FL
Lloyd Parker, NASA, SF, J. F. Kennedy Space Center, FL
George M. Marmaro, NASA, MD-ENV, J. F. Kennedy Space Center, FL
W. A Riehl, Marshall Space Flight Center, NASA, EH31, Marshall SFC, AL
W. C. Pitts, NASA, STPM, Ames Research Center, Moffett Field, CA
J. J. Givens, Ames Research Center, Moffett Field, CA
R. Corridan, Ames Research Center-NASA, Moffett Field, CA
Kenneth Sutton, Langley Research Center, NASA, Hampton, VA
Gerald D. Walberg, Langley Research Center, NASA, Hampton, VA
G. J. Schaefer, Jr., Lewis Research Center, NASA, LeRc-501, Cleveland, OH
R. C. Turkolu, TRW, Defense and Space Systems Group, Redondo Beach, CA
D. Eaton, European Space Research and Technology Centre, Zwarteweg 62, Njordwijk, The Netherlands
Dr. Ralph R. Fullwood, Science Applications, Inc., Palo Alto, CA
D. Glenn, The Aerospace Corporation, Los Angeles, CA
Dr. William Ailor, The Aerospace Corporation, Los Angeles, CA
T. Carter, Nuclear Regulatory Commission, Washington, DC
C. R. Chappell, Nuclear Regulatory Commission, Washington, DC
D. E. Janes, U. S. Environmental Protection Agency, Washington, DC
D. Eagan, Office of Radiation Programs, Washington, DC
James Boland, Argonne National Laboratory-West, Idaho Falls, ID
N. Elsner, General Atomics, San Diego, CA
R. F. Abbey, Naval Research Laboratory, Washington, DC
Charles Salisbury, Naval Ocean Systems Center, San Diego, CA
Dr. Herbert Weiss, Naval Ocean Systems Center, San Diego, CA
R. Cuddihy, IIT Research Institute, Chicago, IL
J. F. Park, Pacific Northwest Laboratory, Richland, WA
Thomas M. Beasley, Oregon State University, Newport, OR
Jackson O. Blanton, Skidaway Inst. of Oceanography, Savannah, GA
Martha Scott, Texas A&M University, College Station, TX
H. James Simpson, Columbia University, Palisades, NY
S. S. Hecker, Los Alamos National Laboratory, Los Alamos, NM
R. N. R. Mulford, Los Alamos National Laboratory, Los Alamos, NM
J. Birely, Los Alamos National Laboratory, Los Alamos, NM
S. E. Bronisz, Los Alamos National Laboratory, Los Alamos, NM
W. Stark, Los Alamos National Laboratory, Los Alamos, NM
R. W. Zocher, Los Alamos National Laboratory, Los Alamos, NM
J. A. Pattillo, Los Alamos National Laboratory, Los Alamos, NM
E. M Wewerka, Los Alamos National Laboratory, Los Alamos, NM
T. C. Wallace, Los Alamos National Laboratory, Los Alamos, NM
T. K. Keenan, Los Alamos National Laboratory, Los Alamos, NM
C. M. Seabourn, Los Alamos National Laboratory, Los Alamos, NM
P. Wagner, Los Alamos National Laboratory, Los Alamos, NM